BOREAL ENVIRONMENT RESEARCH 28: 1–13
ISSN 1797-2469 (online)

Helsinki 25 January 2023

Direct link between the characteristics of atmospheric new particle formation and Continental Biosphere-Atmosphere-Cloud-Climate (COBACC) feedback loop

Markku Kulmala[1,2,3*], Runlong Cai[1], Ekaterina Ezhova[1], Chenjuan Deng[1,4], Dominik Stolzenburg[1], Lubna Dada[1,5], Yishuo Guo[1,2], Chao Yan[1,2,3], Otso Peräkylä[1], Anna Lintunen[1,6], Tuomo Nieminen[1,6], Tom V. Kokkonen[1], Nina Sarnela[1], Tuukka Petäjä[1,3] and Veli-Matti Kerminen[1,3]

[1)] *Institute for Atmospheric and Earth System Research (INAR) / Physics, Faculty of Science, University of Helsinki, Finland*
*(*corresponding author's e-mail: markku.kulmala@helsinki.fi)*
[2)] *Aerosol and Haze Laboratory, Beijing Advanced Innovation Center for Soft Matter Sciences and Engineering, Beijing University of Chemical Technology (BUCT), Beijing, China*
[3)] *Joint International Research Laboratory of Atmospheric and Earth System Sciences, School of Atmospheric Sciences, Nanjing University, Nanjing, China*
[4)] *State Key Joint Laboratory of Environment Simulation and Pollution Control, School of Environment, Tsinghua University, Beijing, China*
[5)] *Laboratory of Atmospheric Chemistry, Paul Scherrer Institute, 5232 Villigen, Switzerland*
[6)] *Institute for Atmospheric and Earth System Research (INAR) / Forest Sciences, Faculty of Agriculture and Forestry, University of Helsinki, Finland*

Received 16 Sep. 2022, final version received 25 Nov. 2022, accepted 25 Nov. 2022

Kulmala M., Cai R., Ezhova E., Deng C., Stolzenburg D., Dada L., Guo Y., Yan C., Peräkylä O., Lintunen A., Nieminen T., Kokkonen T. V., Sarnela N., Petäjä T. & Kerminen V.-M. 2023: Direct link between the characteristics of atmospheric new particle formation and Continental Biosphere-Atmosphere-Cloud-Climate (COBACC) feedback loop. *Boreal Env. Res.* 28: 1–13.

We investigated the role of atmospheric new particle formation (NPF) in the Continental Biosphere-Atmosphere-Cloud-Climate (COBACC) feedback mechanism, particularly the influences of NPF on condensation sink and particle number and cloud condensation nuclei (CCN) concentrations. Using atmospheric observations at the SMEAR II station in Hyytiälä, Finland, we showed that the growth rates of particles originating from NPF are relatively constant, depending only weakly on low-volatility vapor concentrations and having no apparent connection with the strength of NPF or the level of background pollution. We then constrained aerosol dynamic model simulations with these observations. We showed that under conditions typical for the boreal forest atmosphere, even the weakest NPF with a relatively low particle formation rate of 0.01 cm^{-3} s^{-1} at 5 nm (J_5) is capable of enhancing the condensation sink (CS) to values larger than 0.001 s^{-1} after two days of particle growth. When J_5 lies in a typical NPF range between about 0.1 and 0.5 cm^{-3} s^{-1} at SMEAR II, the growing-mode particles originating from NPF tend to dominate the total CS at this station. Increases in CS associated with NPF further increase the ratio of diffuse radiation to global radiation under clear sky by factors between about 1.5 and 2 at SMEAR II, which boosts the forest gross primary production and enhances forest carbon sink. Furthermore, when

Editor in charge of this article: Antti Arola

J_5 is larger than about 0.1 cm^{-3} s^{-1}, NPF frequently produces particle number concentrations larger than 1000 cm^{-3} into the size range relevant for cloud droplet activation. We conclude that outside the late autumn and winter periods when the frequency of NPF is low at SMEAR II, NPF followed by subsequent particle growth is able to give a dominant contribution to both CS and CCN concentration — the two most relevant aerosol-related quantities in the COBACC feedback mechanism. With some reservation, the same conclusion is likely to hold over large regions in the boreal forest zone.

Introduction

Atmospheric aerosol particles associated with emissions from the nature are central players in several potentially large climate feedbacks that operate in the Earth system, as demonstrated with help of global-scale model experiments (e.g. Scott *et al.* 2018, Sporre *et al.* 2019, Fung *et al.* 2022, Zhou *et al.* 2022). In the terrestrial biosphere, an important framework for such feedbacks is the Continental Biosphere-Atmosphere-Cloud-Climate (COBACC) feedback mechanism outlined by Kulmala *et al.* (2014). It describes the response of the terrestrial biosphere to increased CO_2 concentrations and ambient temperatures, and the consequent chain of processes leading to an increased carbon uptake by the biosphere and various radiative effects that tend to cool the overlaying atmosphere. As such, the COBACC feedback mechanism can be considered as negative feedback in the climate system.

In the process level, higher temperatures cause increased emissions of biogenic volatile organic compounds (BVOCs) from the biosphere to the atmosphere (e.g. Tingey *et al.* 1980, Lappalainen *et al.* 2009, Laothawornkitkul *et al.* 2009). Atmospheric oxidation of BVOCs produces low-volatility compounds that contribute to the formation and growth of atmospheric aerosol particles (Ehn *et al.*, 2014, Bianchi *et al.*, 2016, Heinritzi *et al.* 2020). An increased atmospheric aerosol loading originating from BVOCs has two major effects, resulting in two separate loops in the overall feedback mechanism. First, it increases the diffuse fraction of solar radiation entering the Earth's surface, or canopies in the terrestrial biosphere, which enhances ecosystem photosynthesis (e.g. Gu *et al.* 2002, Ezhova *et al.* 2018, Zhou *et al.* 2021), i.e., carbon uptake by the terrestrial biosphere. Second, it causes a larger fraction of incoming solar radiation to be scattered back to space via aerosol-cloud interactions tied with the subpopulation of aerosol particles able to act as cloud condensation nuclei (CCN), as well as via aerosol-radiation interactions (e.g. Lihavainen *et al.* 2009, Paasonen *et al.* 2013, Yli-Juuti *et al.* 2021). Kulmala *et al.* (2020) estimated that influences of forests on aerosols, clouds and carbon uptake (CarbonSink+) may outweigh the warming effect of forest albedo compared with e.g. grass lands (Betts 2000), at least over Northern Europe and the European parts of Russia.

The COBACC feedback mechanism, or some parts of it, have been studied using both atmospheric observations (Paasonen *et al.* 2013; Kulmala *et al.* 2014, Ezhova *et al.* 2018, Yli-Juuti *et al.* 2021, Petäjä *et al.* 2022) and large-scale model simulations (Rap *et al.* 2018, Sporre *et al.* 2019). A crucial component of both loops of the COBACC feedback is atmospheric new particle formation (NPF) and subsequent growth of the newly formed particles to larger sizes, leading to increased aerosol particle number (N) and CCN concentrations as well as increased values of condensation sink (CS). Here, we investigate how the characteristics of NPF influences the COBACC feedback based on aerosol dynamic modeling and data analysis. We hypothesize that NPF plays a dominant role in forming the aerosol population relevant to the COBACC feedback in a boreal forest environment, excluding most of the wintertime when this ecosystem shows little biogenic activity. To test our hypothesis, we first use a model to quantify how sensitive N and CS are to the characteristics of NPF and pre-existing background particle population. We then investigate consequences of these sensitivities to the observed diffuse fraction and carbon uptake of the forest on one hand, and to the observed CCN and cloud droplet populations on the other hand,

at one representative boreal forest site — the SMEAR II station in Hyytiälä, Finland. Finally, we briefly discuss the implications of our finding to the COBACC feedback over the whole boreal forest environment.

Methods

Particle number size distributions have been continuously measured at the SMEAR II station in Hyytiälä, Finland, since 1996 (Hari and Kulmala 2005).

Instrumentation

Particle number size distributions in a wide size range of particle diameters (2.5–1000 nm) were measured using a Neutral cluster and Air Ion Spectrometer (NAIS, 2.5–42 nm; Airel Ltd., Mirme and Mirme 2013, Manninen *et al.* 2016) and a custom-built Differential Mobility Particle Sizer (DMPS, 6–1000 nm, Keady *et al.* 1983, Aalto *et al.* 2001). The DMPS data from years 1996–2020 was downloaded from SmartSMEAR database (https://smear.avaa.csc.fi/, last access: 14 September 2022).

The concentrations of condensable vapors, i.e., sulfuric acid and highly oxygenated organic molecules (HOMs, see Bianchi *et al.* 2019) were measured using a nitrate-based Chemical Ionization Atmospheric Pressure interface Time-of-Flight mass spectrometer (CI-APi-ToF, Aerodyne Research Inc.). The configuration of this instrument was described in detail in our previous studies (Yan *et al.* 2016, Bianchi *et al.* 2017, Zha *et al.* 2018). The direct calibration of sulfuric acid used the same method as in Kürten *et al.* (2012), where known amounts of gaseous sulfuric acid were produced via SO_2 oxidation by OH radical. We used in total 50 months of data on the concentrations of condensable vapors from the years 2013–2020. The total concentration of condensable vapours was obtained by summing up the concentration of sulfuric acid and highly oxygenated organic molecule monomers and dimers (using unit mass resolution data of m/z 290–620 Th).

For solar radiation, we used data measured at the SMEAR II station from 2008–2010. This period was selected, following Ezhova *et al.* (2018) because it provides enough points for statistical analysis and covers the range of CS typical for SMEAR II, from a little less than 0.001 s^{-1} to a little more than 0.01 s^{-1}. A Reemann TP-3 pyranometer with a shading ring was used for the measurements of diffuse radiation and Middleton SK08 pyranometer — for the measurements of global radiation from 2008–2009 (SMEAR II data, https://smear.avaa.csc.fi/). In 2010, a Delta-T BF3/BF5 sunshine sensor was used for the measurement of diffuse photosynthetically active radiation (PAR), and a Li-Cor Li-190SZ quantum sensor was used for the measurements of PAR.

Data analysis

Particle growth rates (GR) in size bins 3–7 nm and 7–15 nm were calculated using the maximum concentration method based on NAIS and DMPS data (Kulmala *et al.* 2012). In this method, the time of the concentration maximum in each bin of the measured size distribution is determined, and the value of GR is obtained from the slope of the linear fit of particle sizes as a function of these times. The value of condensation sink (CS) was calculated from the DMPS data assuming H_2SO_4 as the condensing vapor, as illustrated by Kulmala *et al.* (2005).

The ratio between the diffuse radiation and global radiation depends on the aerosol population represented here by CS. We did not consider aerosol-cloud interactions and thus concentrated on clear-sky days. Similar to Ezhova *et al.* (2018), we used the data measured at 18 m above the ground level at the SMEAR II in 2008–2010, i.e., we work with the broadband radiation in the spectral range between 0.3 and 4.8 μm in 2008–2009 and PAR in the spectral range between 0.3 and 0.7 μm in 2010, which was recalculated to the diffuse fraction of broadband radiation as demonstrated in Ezhova *et al.* (2018). The data are from the maximum growing season (June-August), averaged over half an hour.

We compared measured and modelled radiation to find clear-sky data. Modelling was performed with clear-sky model Solis (Ineichen 2008). Following Ezhova *et al.* (2018), we used the following criteria to find clear-sky data:

$$\frac{R_{g,meas}}{R_{g,\mathrm{mod}}} \geq 0.9; 0.8 \leq \frac{R_{d,meas}}{R_{d,\mathrm{mod}}} \leq 1.2. \quad (1)$$

Here, $R_{\mathrm{g,meas}}$ is the measured global radiation, $R_{\mathrm{g,mod}}$ is the modeled global radiation, $R_{\mathrm{d,meas}}$ is the measured diffuse radiation, and $R_{\mathrm{d,mod}}$ is the modeled diffuse radiation.

Model description

A box model was used to investigate how atmospheric NPF affects the COBACC feedback loop. We mainly focus on the number concentration, condensation sink, and particulate mass contributed by NPF after subsequent growth as responses to particle formation and growth rates. To minimize the uncertainties in the particle survival probability, especially for new particles close to the cluster size (Kulmala *et al.* 2017), the initial size of new particles in most parts of this study was taken as 5 nm. The total number concentration of newly formed particles was computed using the integration of J_5 with respect to time. During the growth, particles are scavenged by coagulation to a background particle population. These background particles were assumed to have an initial diameter of 100 nm and to grow with a rate of 2.08 nm/h to, reaching 200 nm after 48 h of model simulation, consistent with typical geometric diameters of accumulation mode particles at the SMEAR II station (Mäkelä *et al.* 2000). The size-dependent coagulation sink (CoagS) is calculated from the condensation sink (CS) for sulfuric acid using a power-law size dependency of CoagS on particle diameter with exponent value of –1.7, which is typical for the boreal forest environment (Kerminen and Kulmala, 2002; Lehtinen *et al.* 2007). The self-coagulation of newly formed particles is also accounted for, which may contribute to the total CS at high formation rates. Particle losses due to deposition are neglected. Using J_5, CS, and GR, we numerically solve the number concentration of new particles as a function of the growing particle size by tracking the growth trajectory of these new particles.

The number concentration of new particles was converted to the corresponding mass concentration and the contribution to CS, with the mass and CS mean diameters computed using the Hatch-Choate equation (Hatch and Choate 1929):

$$d_{mean} = d_p \exp\left\{(m+0.5)[\ln(\sigma_{\mathrm{geo}})]^2\right\}, \quad (2)$$

where the growing mode is assumed to follow a lognormal distribution and d_{mean} is the mode mean diameter. The value of m is 3 for mass and it is a certain value as a function of d_{p} ranging between 1 and 2 for CoagS. σ_{geo} is the geometric standard deviation of the growing mode. σ_{geo} is assumed to be 1.4 for the most parts in this study. We also compared the results with σ_{geo} values of 1.2, 1.4, and 1.7 to see how sensitive our simulations are to σ_{geo}. In this way, we account for the influences of the dispersity of new particles on CS. More details of this box model can be found in Kulmala *et al.* (2022a).

Results and Discussion

We start our analysis by constraining the growth rate, GR, of newly formed particles for our model simulations based on long-term observations. The value of GR is an essential parameter for our purposes, since it dictates the survival probability of particles formed by atmospheric NPF (McMurry and Friedlander 1979, Kerminen and Kulmala 2002, Pierce and Adams 2007) and thereby determines the fraction of a newly formed particle population that contributes to either secondary particle loading or cloud condensation nuclei (CCN) concentration. When combining data from multiple NPF events together (Figs. 1 and 2), we can see that the value of GR increases slightly with an increasing particle size, has practically no dependence on the strength of a NPF event (Fig. 1), has a relatively weak dependence on the concentration of the potential condensable vapors H_2SO_4 and HOMs (Fig. 2), and depends only weakly on the level of background pollution as measured

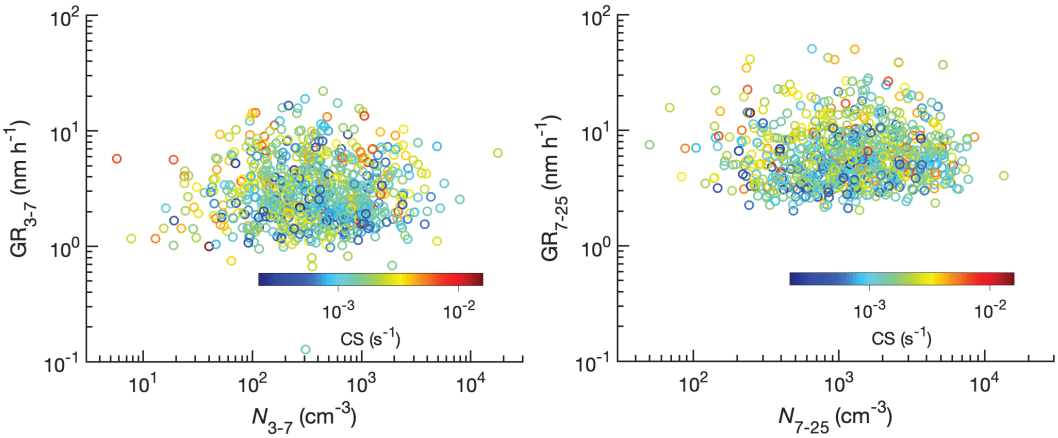

Fig. 1. Growth rates of 3–7 nm (left panel) and 7–25 nm (right panel) particles as a function of the total particle number concentration in the corresponding size ranges, color-coded by condensation sink (CS). The daily particle concentration and CS are average values from 08:00 to 16:00, since this is time window in which the formation of new particles and their subsequent growth typically takes place in the SMEAR II station.

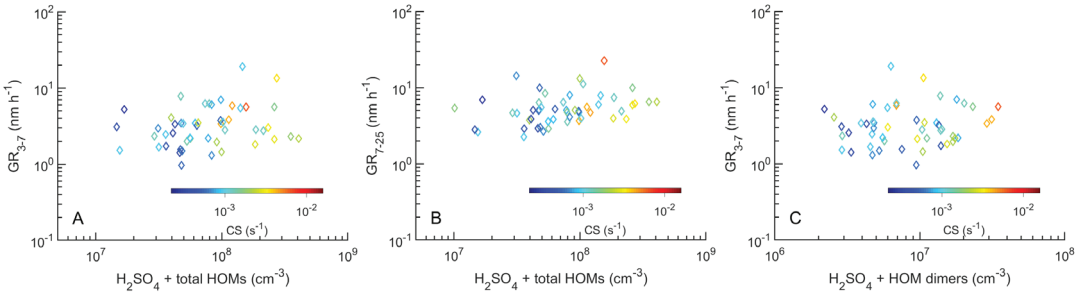

Fig. 2. Growth rates of (**a**) 3–7 nm and (**b**) 7–25 nm particles as a function of the sulfuric acid + total HOM concentration, and (**c**) growth rates of 3–7 nm particles as a function of the sulfuric acid + HOM dimer concentration, color-coded by condensation sink (CS). The daily concentrations of condensable vapors and CS are average values from 08:00 to 16:00.

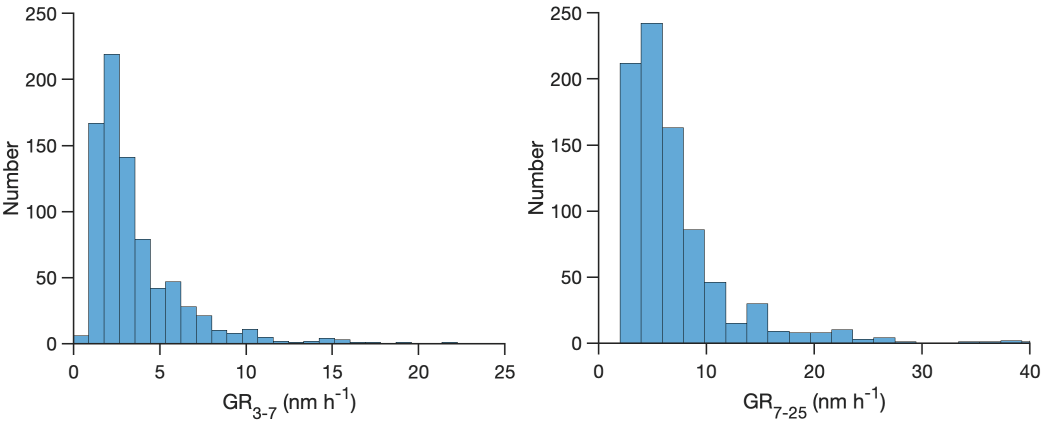

Fig. 3. Histograms of the growth rates of 3–7 nm (left panel) and 7–25 nm (right panel) particles corresponding to the data presented in Fig. 1.

by the condensation sink. These features, and especially the relatively small variability of GR (Fig. 3, Table 1), are surprisingly similar to what we observed in a megacity like Beijing, which is a completely different atmospheric environment (Deng *et al.* 2021, Kulmala *et al.* 2022a,).

Earlier studies made at the SMEAR II station show that the increase of GR with an increasing particle size (Fig. 1) is strongest for the smallest particles (< a few nm in diameter), and that this feature is most prominent during periods with large biogenic aerosol precursor emissions, especially monoterpenes, to the measured air masses (Hirsikko *et al.* 2005, Yli-Juuti *et al.* 2011, Paasonen *et al.* 2018). Mohr *et al.* (2019) could explain spring-time growth by the measurement of gas-phase organics, but they also found a very limited variability in the growth rates. Our dataset including data from all seasons demonstrates that there is overall a weak dependence of GR on the concentration of H_2SO_4 and HOMs. While at smaller sizes (3–7 nm, Fig. 2a) the expected GR from measured vapor concentrations might be overestimated as not all HOM might be of low enough volatility at all temperatures to overcome the enhanced Kelvin-barrier (Stolzenburg *et al.* 2018), at larger sizes (7–25 nm) all HOMs should be condensable, but again we do not find a strong correlation between vapor concentrations and the observed GR (Fig. 2b). This also holds if we constrain the low volatility vapors to only include H_2SO_4 and HOM dimers (with number of carbon atoms > 10), which should be condensable onto > 3 nm particles under almost all conditions (Fig. 2c). This indicates that the growth of newly formed particles to larger sizes is very unlikely to be solely driven by condensation of the low-volatility vapors considered here. Multiphase reactions involving more volatile vapors or rate-limiting effects in condensational growth of low-volatility vapors might be important to the growth process. For a more detailed discussion on this topic, see Kulmala *et al.* (2022a).

We may conclude that although there seems to be strong association between GR and biogenic aerosol precursor vapors, we do not have a clear understanding on how the behavior of GR depends on concentrations of vapors of different volatility at our site. With a lack of proper tools to link GR with aerosol precursor vapors, we decided to use a fixed value of GR in our model simulations. To minimize errors resulting from this approximation, especially due to the apparent size dependency of GR, we will start all the simulations from a point when newly formed particles have already reached 5 nm in diameter. This choice has the additional advantage that we can initiate simulations using the observed formation rate of 5 nm particles, J_5, which is a much better-constrained quantity than J_5 derived from an observed formation rate of 1–2 nm clusters accompanied by simulated growth of these clusters to 5 nm.

Figure 4 shows an example case of the conducted simulations, with the selected initial conditions being representative of those observed during typical NPF events at SMEAR II (Nieminen *et al.* 2014, 2018, Dada *et al.* 2017, Table 1). In this case, particles formed originally by NPF reach CCN sizes (> 50-100 nm in diameter, Kerminen *et al.* 2012) after about 20 to 40 hours of their growth, consistent with direct CCN measurements following NPF at this site (Sihto *et al.* 2011) and reported evolution of particle number size distributions based on a time-over-land analysis made for air masses entering the site (Petäjä *et al.* 2022). The total particle number concentration of the growing mode reaches a few thousand cm^{-3} and decreases by a factor of 2–3 during the 2-day simulation due to coagulation of these particles with the pre-existing larger particles. For this background particle population (initial $CS_{background}$ = 0.001 s^{-1} and GR = 2.08 nm/h), the

Table 1. Statistical values of the aerosol particle growth rates (GR) in Fig. 1.

Size range	GR (nm/h)					Correlation parameters	
	Median	25%	75%	10%	90%	*r*	*p*
3-7 nm	2.7	1.9	4.3	1.4	6.8	0.0168	0.63531
7–25 nm	5.6	4.0	8.3	3.2	13.4	0.0255	0.45909

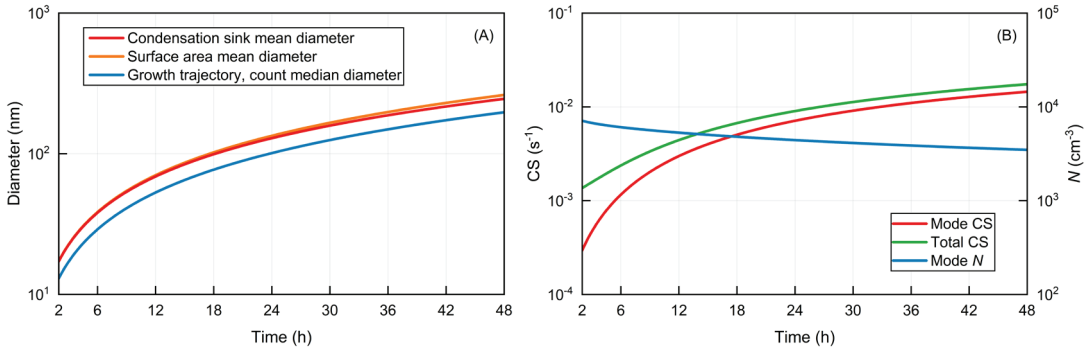

Fig. 4. Simulated growth of newly formed particles. Panel A shows different diameters of the growing mode during the model experiment, and panel B shows the corresponding total particle number concentration (N) and condensation sink (CS). The model inputs are: J_5 = 0.5 cm^{-3} s^{-1}, duration of NPF = 5 h, GR = 4 nm/h for the growing mode and GR = 2.08 nm/h for background particles, geometric standard deviation (σ_{geo}) of the growing mode = 1.4, CS = 0.001 s^{-1} for the background aerosol population, and CS/GR = 0.9 nm^{-1}.

growing mode starts to dominate the total CS already after about 10 h of simulation time, and the total value of CS exceeds 0.01 s^{-1} before the end of the simulation. These results depend only moderately on the assumed width of the growing mode (Table 2), so the simulations presented later in this paper were all conducted by assuming σ_{geo} = 1.4.

We next investigate the sensitivity of the simulation result to the key variables affecting the dynamics of this system. Figure 5 shows that for initial $CS_{background}$ = 0.001 s^{-1}, NPF contributes little to the total particle number concentration or to the total CS during the 48-h simulation unless the formation rate of 5 nm particles exceeds 0.01 cm^{-3} s^{-1}. With increasing values of J_5, these contributions increase rapidly so that for J_5 larger than 0.1 cm^{-3} s^{-1}, the number concentration of particles in the growing mode (N) becomes larger than 1000 cm^{-3} and the growing mode gives a dominant contribution to the total CS. Figure 6 demonstrates that the growth rate of newly formed particles has the largest effects on N and CS when GR is small. This is because the survival probability of growing particles against coagulation scavenging decreases rapidly with their decreasing growth rate, the limiting value of GR being about 3–4 nm/h under the conditions assumed in Fig. 6. For very low values of GR, newly formed clusters will not survive from coagulation scavenging at all, so that NPF will not contribute to either N or CS.

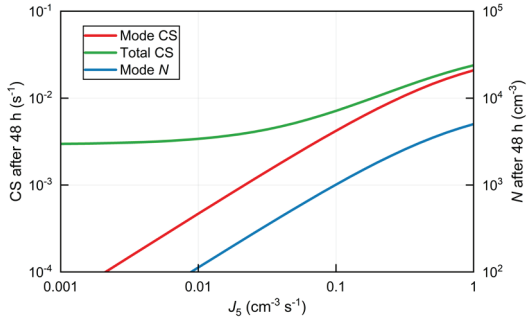

Fig. 5. Total particle number concentration (N) and condensation sink (CS) of the growing mode, along with total CS, after 48 h of simulation tie as function of the formation rate of 5-nm particles, J_5. The other model inputs are the same as in Fig. 4.

Table 2. N and total CS after 48 h for different values of the geometric standard deviation (σ_{geo}) of the growing mode. Similar to the simulations in Fig. 4, J_5 = 0.5 cm^{-3} s^{-1}, duration of NPF = 5 h, GR = 4 nm/h, CS = 0.001 s^{-1} and CS/GR = 0.9 nm^{-1}.

	σ_{geo} = 1.2	σ_{geo} = 1.4	σ_{geo} = 1.7
N (cm^{-3})	4100	3700	2800
CS (s^{-1})	0.015	0.016	0.019

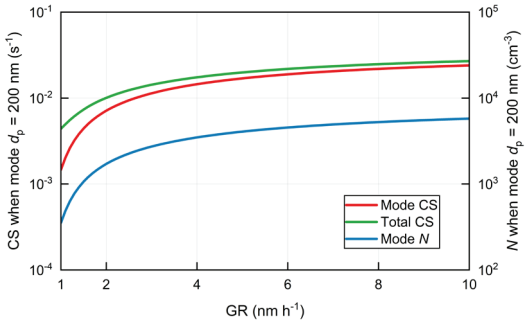

Fig. 6. Total particle number concentration (N) and condensation sink (CS) of the growing mode, along with total CS, after 48 h of simulation tie as function of the growth rate of the growing mode, GR. The other model inputs are the same as in Fig. 4. Note: the ending diameter is the same (200 nm) for different values of GR, while the ending time varies (48 h when GR = 4 nm/h).

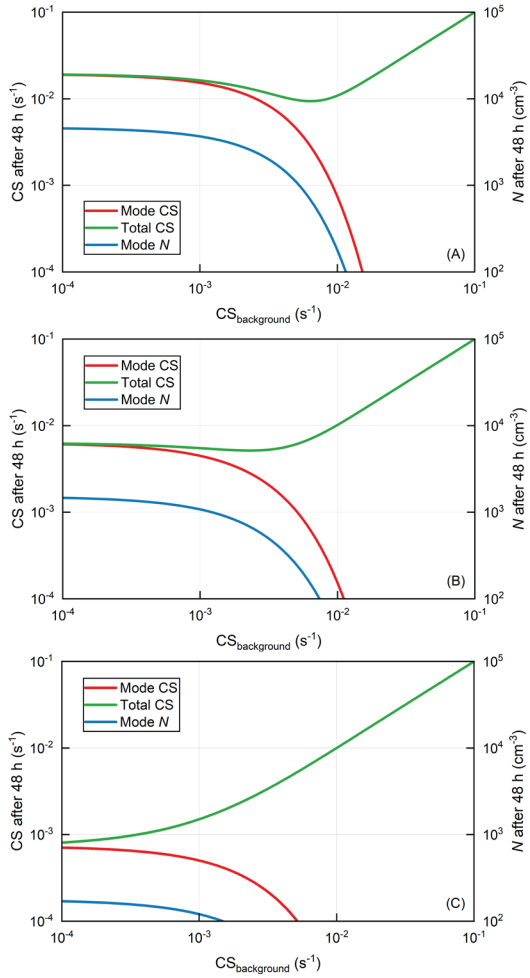

Fig. 7. Total particle number concentration (N) and condensation sink (CS) of the growing mode, along with total CS, after 48 h of simulation time as function of the CS of the background particle population, $CS_{background}$, and for J_5 = (**a**) 0.5, (**b**) 0.1 and (**c**) 0.01 cm^{-3} s^{-1}. $CS_{background}$ is assumed to be constant over time. The other model inputs are the same as in Fig. 4.

Similar to low values of GR, high levels of background particle pollution tend to suppress atmospheric NPF (e.g. Kulmala *et al.* 2017, Deng *et al.* 2021). Figure 7 shows how N and CS behave as a function of the background aerosol pollution as measured by $CS_{background}$. We may see that for both typical (J_5 = 0.5 cm^{-3} s^{-1}) and weak (J_5 = 0.1 cm^{-3} s^{-1}) NPF events observed at SMEAR II (for the variability of J, see Nieminen *et al.* 2014, 2018, Dada *et al.* 2017), the contribution of NPF to CS (and N) after the 48-h simulation remain large for $CS_{background}$ up to about 0.005-0.01 s^{-1}. This is very close to the limiting value range of CS above which NPF has not been observed to take place at SMEAR II (Dada *et al.* 2017). Kulmala *et al.* (2022b) identified recently so-called "quiet NPF", i.e., clustering and subsequent growth of these clusters to larger sizes that occur during the days traditionally classified as non-event days (no NPF taking place). In Fig. 7, such quiet NPF corresponds to the case with J_5 = 0.01 cm^{-3} s^{-1}. We may see that although the particle number concentration of the growing mode remains rather low following quiet NPF, this phenomenon gives a significant contribution to CS for $CS_{background}$ up to about 0.001 s^{-1}.

The simulations performed above demonstrate that atmospheric NPF followed by particle growth is capable of giving a dominant contribution to the total condensation sink of the aerosol population observed at SMEAR II under a variety of atmospheric conditions. A typical value range of CS resulting from atmospheric NPF lies between about 0.001 and 0.01 s^{-1} after 2 days of particle growth, even though also values up to about 0.02 s^{-1} appear possible. Figure 8 shows the ratio between the diffuse and global radiation under clear sky, R_d/R_g, as a function of CS as observed using direct measurements at SMEAR II. We may see that for the CS value range expected to result from atmospheric NPF (0.001–0.02 s^{-1}), the value of R_d/R_g increases from approximately 0.10 corresponding to low

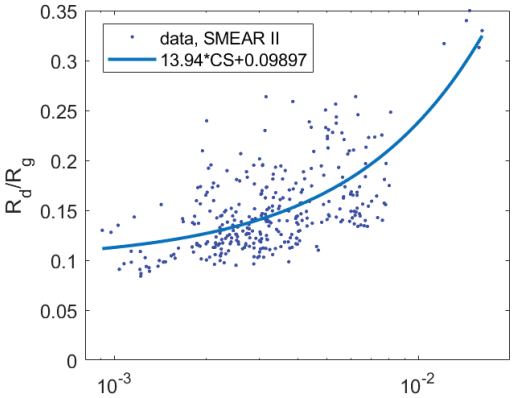

Fig. 8. The ratio between the diffuse and global radiation as a function of CS observed at SMEAR II.

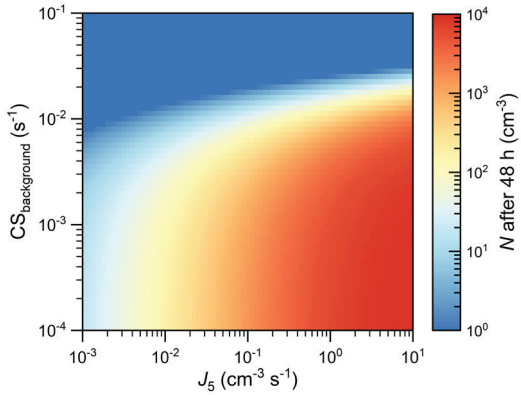

Fig. 9. Particle number concentrations in the growing mode after 48 h of simulations as function of $CS_{background}$ and J_5. $CS_{background}$ is assumed to be constant over time. The other model inputs are the same as in Fig. 4.

aerosol loadings up to about 0.25–0.3 for the highest values of CS. According to Ezhova *et al.* (2018), such an increase in R_d/R_g leads to a 6% increase in the gross primary production (GPP) at SMEAR II (i.e. the impact of increasing light use efficiency on GPP overrules the impact of decreasing global radiation on GPP). In some coniferous forests at high latitudes and mixed forests at middle latitudes, the increase in GPP caused by such an increase in R_d/R_g has been shown to be even higher (Ezhova *et al.* 2018).

Finally, we have a look at what implications our simulation results have on the other loop of the COBACC feedback that involves CCN and droplet number concentrations. Figure 9 summarizes the combined effects of J_5 and $CS_{background}$ on the total particle number concentration of the growing mode after 48 h of the simulation time. We can see that N remains below 100 cm^{-3} when J_5 is smaller than about 0.01 cm^{-3} s^{-1}, corresponding to quiet NPF (Kulmala *et al.* 2022b), or when $CS_{background}$ is larger than about 0.01 s^{-1} so that the particles in the growing mode will be efficiently scavenged by coagulation. On the other hand, when J_5 is larger than 0.1 cm^{-3} s^{-1} and CS remains smaller than about 0.002-0.003 s^{-1}, N exceeds 1000 cm^{-3}. Long-term measurements at SMEAR II indicate that the monthly-median particle number concentration varies between about 200 and 600 cm^{-3} in the accumulation mode and between about 400 and 1100 cm^{-3} in the Aitken mode, while the monthly-median CS varies between about 0.002 and 0.004 s^{-1} (Neefjes *et al.* 2022). The median CS diameter of the particle population at SMEAR II was reported to be 100 nm (Dal Maso *et al.* 2008), comparable to that reached in our simulations (Fig. 4). When looking at originally clean air masses entering the boreal forest zone and then transported to SMEAR II for about two days, measured CCN concentrations were found to be between about 200 and 300 cm^{-3} at the 0.2% supersaturation and between about 600 and 1000 cm^{-3} at the 1.0% supersaturation, whereas retrieved cloud droplet number concentrations were between about 500 and 700 cm^{-3} (Petäjä *et al.* 2022). These observations suggest that, consistent with in situ observations of clouds at another boreal forest site (Komppula *et al.* 2005), activation of accumulation mode and some fraction of the Aitken mode particles constitute the cloud droplet population above SMEAR II. Our simulation results in Figs. 4 and 8 suggest that when occurring, NPF followed by two days of particle growth can fully explain observed CCN and cloud droplet number concentrations in observed at SMEAR II.

Conclusions

We investigated how the characteristics of NPF influences the COBACC feedback based on aerosol dynamic modeling and analysis of atmospheric observations. Using long-term observations made at the SMEAR II station in Hyytiälä,

Finland, we showed that the growth rates of particles originating from NPF are relatively constant, depending only weakly on the major low-volatility vapors, H_2SO_4 and HOMs, and having no apparent connection with the strength of NPF or the level of background pollution.

Our model simulations demonstrate that typical NPF events observed at the SMEAR II station in Hyytiälä, Finland, followed by two days of particle growth, are capable of producing the dominant fractions of both the CS and CCN population at this site. Since the CS and CCN concentrations are the most relevant aerosol-related variables in the COBACC feedback mechanism (Kulmala *et al.* 2014, Ezhova *et al.* 2018), this means that the role of NPF in the COBACC feedback depends essentially on how the frequency of NPF compares with the typical atmospheric lifetime of the sub-population of aerosol particles determining CS and CCN concentration. Furthermore, the formation rate of 5 nm particles defines how important the contribution of NPF to CCN and CS production is. At SMEAR II, the monthly-median NPF event frequency varies between about 15% and 40% from March until about October, i.e. outside the late autumn and winter period (Neefjes *et al.* 2022). Estimated lifetimes of aerosol particles at sizes most relevant for CS and CCN range from a couple of days up to about a week in atmospheric boundary layers (e.g. Williams *et al.* 2002, Feichter and Leisner 2009), so we may conclude that NPF followed by subsequent growth of the newly formed particles is able to give a significant contribution to both CS and CCN concentration at this site outside the late autumn and winter period.

Kerminen *et al.* (2018) summarized the basic characteristics of NPF in the boreal forest zone based on investigations made at 12 different sites in this region. The median particle formation and growth rates for these sites were equal to 0.4 cm^{-3} s^{-1} and 2.7 nm/h, respectively, comparable with the values used in our model simulations. Taken the typical lifetimes of particles at sizes most relevant for CS and CCN, NPF followed by growth could thereby give a dominant contribution to these quantities over the regions with NPF event frequencies exceeding about 20–30%. Typical NPF event frequencies vary between about 10% and 30% in the boreal forest zone, the lowest frequencies being observed at the northern edge and Siberian part (frequencies down to a few %) of it (Asmi *et al.* 2011, Kyrö *et al.* 2014, Kerminen *et al.* 2018, Wiedensohler *et al.* 2019). This means that conclusions made here for SMEAR II probably hold over large areas in the boreal forest zone. In regions with the lowest NPF frequencies, it might be worth investigating the role of "quiet NPF" that appears as a persistent phenomenon outside periods coved by traditional NPF events (Kulmala *et al.* 2022b).

Acknowledgements: We acknowledge the following projects: ACCC Flagship funded by the Academy of Finland grant number 337549, Academy professorship funded by the Academy of Finland (grant no. 302958), Academy of Finland projects no. 1325656, 311932, 334792, 316114, 325647, 325681, 347782, "Quantifying carbon sink, CarbonSink+ and their interaction with air quality" INAR project funded by Jane and Aatos Erkko Foundation, European Research Council (ERC) project ATM-GTP Contract No. 742206, Samsung PM2.5 SRP, the European Union's Horizon 2020 research and innovation programme Marie Sklodowska-Curie grant agreement no. 895875 ("NPF-PANDA"), the Marie Skłodowska Curie ITN "CLOUD-MOTION" (grant agreement no. 764991), FORCeS (grant agreement no. 821205), and European Union's Horizon Europe research and innovation programme project Non-CO2 Forcers and their Climate, Weather, Air Quality and Health Impacts (FOCI, grant agreement no. 101056783). University of Helsinki support via ACTRIS-HY is acknowledged. Support of the technical and scientific staff in Hyytiälä are acknowledged.

References

Aalto P., Hämeri K., Becker E., Weber R., Salm J., Mäkelä J.M., Hoell C., O'Dowd C.D., Hansson H.-C., Väkevä M., Koponen I.K., Buzorius G. & Kulmala M. 2001. Physical characterization of aerosol particles during nucleation events. *Tellus* 53B: 344–358. 10.3402/tellusb.v53i4.17127, 2001.

Asmi E., Kivekäs N., Kerminen V.-M., Komppula M., Hyvärinen A.-P., Hatakka J., Viisanen Y. & Lihavainen H. 2011. Secondary new particle formation in Northern Finland Pallas site between the years 2000 and 2010. *Atmos. Chem. Phys.* 11: 12959–12972.

Betts R.A. 2000. Offset of the potential carbon sink from boreal forestation by decreases in surface albedo. *Nature* 408: 187–190.

Bianchi F., Garmash O., He X., Yan C., Iyer S., Rosendahl I., Xu Z., Rissanen M.P., Riva M., Taipale R., Sarnela

N., Petäjä T., Worsnop D.R., Kulmala M., Ehn M. & Junninen H. 2017. The role of highly oxygenated molecules (HOMs) in determining the composition of ambient ions in the boreal forest. *Atmos. Chem. Phys.* 17: 13819–13831.

Bianchi F., Kurtén T., Riva M., Mohr C., Rissanen M.P., Roldin P., Berndt T., Crounse J.D., Wennberg P.O., Mentel T.F., Wildt J., Junninen H., Jokinen T., Kulmala M., Worsnop D.R., Thornton J.A., Donahue N., Kjaergaard H.G. & Ehn M. 2019. Highly oxygenated organic molecules (HOM) from gas-phase autoxidation involving peroxy radicals: A key contributor to atmospheric aerosol. *Chem. Rev.* 119: 3472–3509.

Dada L., Paasonen P., Nieminen T., Buenrostro-Mazon S., Kontkanen J., Peräkylä O., Lehtipalo K., Hussein T., Petäjä T., Kerminen V.-M., Bäck J. & Kulmala M. 2017. Long-term analysis of clear-sky new particle formation events and nonevents in Hyytiälä. *Atmos. Chem. Phys.* 17: 6227–6241.

Dal Maso M., Hyvärinen A., Komppula M., Tunved P., Kerminen V.-M., Lihavainen H., Viisanen Y., Hansson H.-C. & Kulmala M. 2008. Annual and interannual variation in boreal forest aerosol particle number and volume concentration and their connection to particle formation. *Tellus* 60B: 495–508.

Deng C., Cai R., Yan C., Zheng J. & Jiang J. 2021. Formation and growth of sub-3 nm particles in megacities: impact of background aerosols. *Faraday Discuss.* 226: 348–363.

Ezhova E., Ylivinkka I., Kuusk J., Komsaare K., Vana M., Krasnova A., Noe S., Arshinov M., Belan B., Park S.-B., Lavrič J.V., Heimann M., Petäjä T., Vesala T., Mammarella I., Kolari P., Bäck J., Rannik Ü., Kerminen V.-M. & Kulmala M. 2018. Direct effect of aerosols on solar radiation and gross primary production in boreal and hemiboreal forests. *Atmos. Chem. Phys*. 18: 17863–17881.

Feichter J. & Leisner T. 2009. Climate engineering: A critical review of approaches to modify the global energy balance. *Eur. Phys. J. Special Topics* 176: 81–92.

Fung K.M., Heald C.L., Kroll J.H., Wang S., Jo D.S., Gettelman A., Lu Z., Liu X., Zaveri R.A., Apel E.C., Blake D.R., Jimenez J.-L., Campuzano-Jost P., Veres P.R., Bates T.S., Shilling J.E. & Zawadowicz M. 2022. Exploring dimethyl sulfide (DMS) oxidation and implications for global aerosol radiative forcing. *Atmos. Chem. Phys.* 22: 1549–1573.

Gu L., Baldocchi D., Verma S.B., Black T.A., Vesala T., Falge E.M. & Dowty P.R. 2002. Advantages of diffuse radiation for terrestrial ecosystem productivity. *J. Geophys. Res. Atmos.* 107: 2–23.

Hatch T. & Choate S.P. 1929. Statistical description of the size properties of non uniform particulate substances. *J. Franklin Institute* 207: 369–387.

Hari P. & Kulmala M. 2005. Station for measuring ecosystem-atmosphere relations (SMEAR II). *Boreal. Env. Res.* 10: 315–322.

Heinritzi M. *et al.* 2020. Molecular understanding of the suppression of new-particle formation by isoprene. *Atmos. Chem. Phys.* 20: 11809–11821.

Hirsikko A., Laakso L., Horrak U., Aalto P.P., Kerminen V.-M. & Kulmala M. 2005. Annual and sie dependent variatoi nof growth rates and ion concentrations in boreal forest. *Boreal. Env. Res*. 10: 357–369.

Ineichen P. 2008. A broadband simplified version of the Solis clear sky model. *Sol. Energy* 82: 758–762.

Keady P.B., Quant F.R. & Sem, G. J. 1983. Differential mobility particle sizer: a new instrument for high-resolution aerosol size distribution measurement below 1 μm. *TSI Quarterly* 9: 3–11.

Kerminen V.-M. – Kulmala M. 2002. Analytical formulae connecting the 'real' and 'apparent' nucleation rate and the nucleus number concentration for atmospheric nucleation events. *J. Aerosol Sci.* 33: 609−622.

Kerminen V.-M., Paramonov M., Anttila T., Riipinen I., Fountoukis C., Korhonen H., Asmi, E., Laakso L., Lihavainen H., Swietlicki E., Svenningsson B., Asmi A., Pandis S. N., Kulmala M. & Petäjä T. 2012. Cloud condensation nuclei production associated with atmospheric nucleation: a synthesis based on existing literature and new results. *Atmos. Chem. Phys.* 12: 12037–12059.

Kerminen V.-M., Chen X., Vakkari V., Petäjä T., Kulmala M. & Bianchi F. 2018. Atmospheric new particle formation and growth: review of field observations. *Environ. Res. Lett.* 13, 103003.

Komppula M., Lihavainen H., Kerminen V.-M., Kulmala M. & Viisanen Y. 2005. Measurements of cloud droplet activation of aerosol particles at a clean subarctic background site. *J. Geophys. Res.* 110, D06204, doi:10.1029/2004JD005200.

Kulmala M., Petäjä T., Mönkkönen P., Koponen I.K., Dal Maso M., Aalto P.P., Lehtinen K.E.J., & Kerminen V.-M. 2005. On the growth of nucleation mode particles: source rates of condensable vapor in polluted and clean environments. *Atmos. Chem. Phys.* 5: 409–416.

Kulmala M., Petäjä T., Nieminen T., Sipilä M., Manninen H.E., Lehtipalo K., Dal Maso M., Aalto P.P., Junninen H., Paasonen P., Riipinen I., Lehtinen K.E.J., Laaksonen A. & Kerminen V.-M. 2012. Measurement of the nucleation of atmospheric aerosol particles. *Nature Protocols* 7: 1651–1667.

Kulmala M., Nieminen T., Nikandrova A., Lehtipalo K., Manninen H.E., Kajos M.K., Kolari P., Lauri A., Petäjä T., Krejci R., Hansson H.-C., Swietlicki E., Lindroth A., Christensen T.R., Arneth A., Hari P., Bäck J., Vesala T. & Kerminen V.-M. 2014. CO_2-induced terrestrial climate feedback mechanism: From carbon sink to aerosol source and back. *Boreal Env. Res.* 19: 122–131.

Kulmala M., Kerminen V.-M., Petäjä T., Ding A. J. & Wang L. 2017. Atmospheric gas-to-particle conversion: why NPF events are observed in megacities? *Faraday Discuss.* 200: 271–288.

Kulmala M., Ezhova E., Kalliokoski T., Noe S., Vesala T., Lohila A., Liski J., Makkonen R., Bäck J., Petäjä T. & Kerminen V.-M. 2020. CarbonSink+ – Accounting for multiple climate feedbacks from forests. *Boreal Env. Res.* 25: 145–159.

Kulmala M., Cai R., Stolzenburg D., Zhou Y., Dada L., Guo

Y., Yan C., Petäjä T., Jiang J. & Kerminen V.-M. 2022a. The contribution of new particle formation and subsequent growth to haze formation. *Environ. Sci.: Atmos.* 2: 352–361.

Kulmala M., Junninen H., Dada L., Salma I., Weidinger T., Thén W., Vörösmarty M., Komsaare K., Stolzenburg D., Cai R., Yan C., Li X., Deng C., Jiang J., Petäjä T., Nieminen T. & Kerminen V.-M. 2022b. Quiet New Particle Formation in the Atmosphere. *Front. Environ. Sci.* 10, 912385, doi: 10.3389/fenvs.2022.912385.

Kürten A., Rondo L., Ehrhart S. & Curtius J. 2012. Calibration of a Chemical Ionization Mass Spectrometer for the Measurement of Gaseous Sulfuric Acid. *J. Phys. Chem. A* 116, 6375–6386. 10.1021/jp212123n.

Kyrö E.-M., Väänänen R., Kerminen V.-M., Virkkula A., Petäjä T., Dal Maso M., Nieminen T., Juhola S., Shcherbinin A., Riipinen I., Lehtipalo K., Keronen P., Aalto P.P., Hari P. & Kulmala M. 2014. Trends in new particle formation in eastern Lapland, Finland: effect of decreasing sulfur emissions from Kola Peninsula. *Atmos. Chem. Phys.* 14: 4383–4396.

Lappalainen H.K., Sevanto S., Bäck J., Ruuskanen T.M., Kolari P., Taipale R., Rinne J., Kulmala M. & Hari P. 2009. Day-time concentrations of biogenic volatile organic compounds in a boreal forest canopy and their relation to environmental and biological factors. *Atmos. Chem. Phys.* 9: 5447–5459.

Laothawornkitkul J., Taylor J.E., Paul N.D. & Hewitt C.N. 2009. Biogenic volatile organic compounds in the Earth system. *New Phytologist* 183: 27–51.

Lehtinen K.E.J., Dal Maso M., Kulmala M. & Kerminen V.-M. 2007. Estimating nucleation rates from apparent particle formation rates and vice versa: Revised formulation of the Kerminen-Kulmala equation. *J. Aerosol Sci.* 38: 988–994.

Lihavainen H., Kerminen V.-M., Tunved P., Aaltonen V., Arola A., Hatakka J., Hyvärinen A. & Viisanen Y. 2009. Observational signature of the direct radiative effect by natural boreal forest aerosols and its relation to the corresponding first indirect effect. *J. Geophys. Res.* 114, D20206, doi:10.1029/2009JD012078.

Mäkelä J.M., Koponen I.K., Aalto P. & Kulmala M. 2000. One-year data of submicron size modes of tropospheric background particle aerosol in Southern Finland. *J. Aerosol Sci.* 31: 595–611.

Manninen H.E., Mirme S., Mirme A., Petäjä T. & Kulmala M. 2016. How to reliably detect molecular clusters and nucleation mode particles with Neutral cluster and Air Ion Spectrometer (NAIS). *Atmos. Meas. Tech.* 9: 3577–3605.

McMurry P.H. & Friedlander S.K. 1979. New particle formation in the presence of an aerosol. *Atmos. Environ.* 13: 1635−1651.

Mirme S. & Mirme A. 2013. The mathematical principles and design of the NAIS – a spectrometer for the measurement of cluster ion and nanometer aerosol size distributions. *Atmos. Meas. Tech.* 6: 1061–1071.

Mohr C., Thornton J.A., Heitto A., Lopez-Hilfiker F.D., Lutz A., Riipinen I., Hong J., Donahue N.M., Hallquist M., Petäjä T., Kulmala M. & Yli-Juuti T. 2019. Molecular identification of organic vapors driving atmospheric nanoparticle growth. *Nature Comm.* 10, 4442.

Neefjes I., Laapas M., Liu Y., Medus E., Miettunen E., Ahonen L., Quelever L., Aalto J., Bäck J., Kerminen V.-M., Lampilahti J., Luoma K., Mäki M., Mammarella I., Petäjä T, Räty M., Sarnela N., Ylivinkka I., Hakala S., Kulmala M., Nieminen T. & Lintunen A. 2022. 25 years of atmospheric and ecosystem measurements in a boreal forest – Seasonal variation and responses to warm and dry years. *Boreal Env. Res.* 27: 1–31.

Nieminen T., Asmi A., Dal Maso M., Aalto, P. P., Keronen P., Petäjä T., Kulmala M. & Kerminen V.-M. 2014. Trends in atmospheric new-particle formation: 16 years of observations in a boreal-forest environment. *Boreal Env. Res.* 19, suppl. B: 191–214.

Nieminen T., Kerminen V.-M., Petäjä T., Aalto P.P., Arshinov M., Asmi E., Baltensperger U., Beddows D. S. C., Beukes J. P., Collins D., Ding A., Harrison R. M., Henzing B., Hooda R., Hu M., Horrak U., Kivekäs N., Komsaare K., Krejci R., Kristensson A., Laakso L., Laaksonen A., Leaitch W. R., Lihavainen H., Mihalopoulos N., Nemeth Z., Nie W., O'Dowd C. D., Salma I., Sellegri K., Svenninsson B., Swietlicki E., tunved P., Ulevicius V., Vakkari V., Vana M., Wiedensohler A., Wu Z., Virtanen A. & Kulmala M. 2018. Global analysis of continental boundary layer new particle formation based on long-term measurements. *Atmos. Chem. Phys.* 18: 14737–14756.

Paasonen P., Asmi A., Petäjä T., Kajos M.K., Äijälä M, Junninen H., Holst T., Abbatt J.P.D., Arneth A., Birmili W., Denier van der Gon H., Hamed A., Hoffer A., Laakso L., Laaksonen A., Leaitch W.R., Plass-Dulmer C., Pryor S. C., Räisänen P., Swietlicki E., Wiedensohler A., Worsnop D.R., Kerminen V.-M. & Kulmala M. 2013. Warming-induced increase in aerosol number concentration likely to moderate climate change. *Nature Geosci.* 6: 438–442.

Paasonen P., Peltola M., Kontkanen J., Junninen H., Kerminen V.-M. & Kulmala M. 2018. Comprehensive analysis of particle growth rates from nucleation mode to cloud condensation nuclei in boreal forest. *Atmos. Chem. Phys.* 18: 12085–12103.

Petäjä T., Tabakova K., Manninen A., Ezhova E., O'Connor E., Moisseev D., Sinclair V. A., Backman J., Levula J., Luoma K., Virkkula A., Paramonov M., Räty M., Äijälä M., Heikkinen L., Ehn M., Sipilä M., Yli-Juuti T., Virtanen A., Ritsche M., Hickmon N., Pulik G., Rosenfeld D., Worsnop D.R., Bäck J., Kulmala M. & Kerminen V.-M. 2022. Influence of biogenic emissions from boreal forests on aerosol-cloud interactions. *Nature Geosci.* 15: 42–47.

Pierce J.R. & Adams P.J. 2007. Efficacy of cloud condensation nuclei formation from ultrafine particles. *Atmos. Chem. Phys.* 7: 1367–1379.

Rap A., Scott C.E., Reddington C.L., Mercado L. Ellis R. J., Garraway S., Evans M.J., Beerling D.J., MacKenzie A.R., Hewitt C.N. & Spracklen D.V. 2018. Enhanced global primary production by biogenic aerosol via diffuse radiation fertilization. *Nature Geosci.* 11: 640–644.

Scott C.E., Arnold S.R. Monks S.A., Asmi A., Paasonen P.

& Spracklen D.V. 2018. Substantial large-scale feedbacks between natural aerosols and climate. *Nature Geosci.* 11: 44–48.

Sihto S.-L., Mikkilä J., Vanhanen J., Ehn M., Liao L., Lehtipalo K., Aalto P.P., Duplissy J., Petäjä T., Kerminen V.-M., Boy M. & Kulmala M. 2011. Seasonal variation of CCN concentrations and aerosol activation properties in boreal forest. *Atmos. Chem. Phys.* 11: 13269–13285.

Sporre M.K., Blichner S.M., Karset I.H.H., Makkonen R. & Berntsen T.K. 2019. BVOC–aerosol–climate feedbacks investigated using NorESM. *Atmos. Chem. Phys*. 19: 4763–4782.

Stolzenburg D., Fischer L., Vogel A.L., Heinritzi M., Schervish M., Simon M., Wagner A. C., Dada L., Ahonen L.R., Amorim A., Baccarini A., Bauer P.S., Baumgartner B., Bergen A., Bianchi F., Breitenlechner M., Brilke S., Buenrostro Mazon S., Chen D., Dias A., Draper D.C., Duplissy J., El Haddad I., Finkenzeller H., Frege C., Fuchs C., Garmash O., Gordon H., He X., Helm J., Hofbauer V., Hoyle C. R., Kim C., Kirkby J., Kontkanen J., Kürten A., Lampilahti J., Lawler M., Lehtipalo K., Leiminger M., Mai H., Mathot S., Mentler B., Molteni U., Nie W., Nieminen T., Nowak J. B., Ojdanic A., Onnela A., Passananti M., Petäjä T., Quéléver L.L.J., Rissanen M.P., Sarnela N., Schallhart S., Tauber C., Tomé A., Wagner R., Wang M., Weitz L., Wimmer D., Xiao M., Yan C., Ye P., Zha Q., Baltensperger U., Curtius J., Dommen J., Flagan R., Kulmala M., Smith J.N., Worsnop D.R., Hansel A., Donahue N.M. & Winkler P.M. 2018. Rapid growth of organic aerosol nanoparticles over a wide tropospheric temperature range. P. Nat. Acad. Sci. USA 115: 9122–9127.

Tingey D., Manning M., Grothaus L. & Burns W. 1980. Influence of light and temperature on monoterpene emission rates from slash pine. *Plant Physiol.* 65: 797–801.

Wiedensohler A., Ma N., Birmili W., Heintzenberg J., Ditas F., Andreae M. O. & Panov A. 2019. Infrequent new particle formation over the remote forest of Siberia. *Atmos. Environ.* 200: 167–169.

Williams J., de Reus M., Krejci R., Fischer H. & Ström J. 2002. Application of the variability-size relationship to atmospheric aerosol studies: estimating aerosol lifetimes and ages. *Atmos. Chem. Phys.* 2: 133–145.

Yan C., Nie W., Äijälä M., Rissanen M.P., Canagaratna M.R., Massoli P., Junninen H., Jokinen T., Sarnela N., Häme S.A.K., Schobesberger S., Canonaco F., Yao L., Prevot A.S.H., Petäjä T., Kulmala M., Sipilä M., Worsnop D.R. & Ehn M. 2016. Source characterization of highly oxidized multifunctional compounds in a boreal forest environment using positive matrix factorization. *Atmos. Chem. Phys*. 16: 12715–12731.

Yli-Juuti T., Nieminen T., Hirsikko A., Aalto P. P., Asmi E., Horrak U., Manninen H. E., Patokoski J., Dal Maso M., Petäjä T., Rinne J., Kulmala M. & Riipinen I. 2011. Growth rates of nucleation mode particles in Hyytiälä during 2003–2009: variation with particle size, season, data analysis methods and ambient conditions. *Atmos. Chem. Phys.* 11: 12865–12886.

Yli-Juuti T., Mielonen T., Heikkinen L., Arola A., Ehn M., Isokääntä S., Keskinen H.-M., Kulmala M., Laakso A., Lipponen A., Luoma K., Mikkonen S., Nieminen T., Paasonen P., Petäjä T., Romakkaniemi S., Tonttila J., Kokkola H. & Virtanen A. 2021. Significance of the organic aerosol driven climate feedback in the boreal area. *Nature Comm.* 12, 5637.

Zha Q., Yan C., Junninen H., Riva M., Sarnela N., Aalto J., Quelever L., Schallhart S., Dada L., Heikkinen L., Peräkylä O., Zou J., Rose C., Wang Y., Mammarella I., Katul G., Vesala T., Worsnop D.R., Kulmala M., Petäjä T. Bianchi F. & Ehn M. 2018. Vertical characterization of highly oxygenated molecules (HOMs) below and above a boreal forest canopy. *Atmos. Chem. Phys.* 18: 17437–17450.

Zhou H., Yue X., Lei Y., Zhang T., Tian C., Ma Y. & Cao Y. 2021. Responses of gross primary productivity to diffuse radiation at global FLUXNET sites. *Atmos. Environ.* 244, 117905.

Zhou H., Yue X., Lei Y., Tian C., Zhu J., Ma Y., Cao Y., Yin X & Zhang Z. 2022. Distinguishing the impacts of natural and anthropogenic aerosols on global gross primary production through diffuse fertilization effect. *Atmos. Chem. Phys.* 22: 693–709.